Active liquid-like behavior of nucleoli determines their size and shape in *Xenopus laevis* oocytes

Clifford P. Brangwynne[a,b,c,1,2], Timothy J. Mitchison[c,d], and Anthony A. Hyman[a]

[a]Max Planck Institute of Molecular Cell Biology and Genetics, Pfotenhauerstrasse 108, 01307 Dresden, Germany; [b]Max Planck Institute for the Physics of Complex Systems, Nöthnitzerstrasse 38, 01187 Dresden, Germany; [c]Marine Biological Laboratory, 7 MBL Street, Woods Hole, MA, 02543; and [d]Department of Systems Biology, Harvard Medical School, 200 Longwood Avenue, Boston, MA, 02115

Edited by Dirk Görlich, Max Planck Institute for Biophysical Chemistry, Göttingen, Germany, and accepted by the Editorial Board January 27, 2011 (received for review November 16, 2010)

For most intracellular structures with larger than molecular dimensions, little is known about the connection between underlying molecular activities and higher order organization such as size and shape. Here, we show that both the size and shape of the amphibian oocyte nucleolus ultimately arise because nucleoli behave as liquid-like droplets of RNA and protein, exhibiting characteristic viscous fluid dynamics even on timescales of <1 min. We use these dynamics to determine an apparent nucleolar viscosity, and we show that this viscosity is ATP-dependent, suggesting a role for active processes in fluidizing internal contents. Nucleolar surface tension and fluidity cause their restructuring into spherical droplets upon imposed mechanical deformations. Nucleoli exhibit a broad distribution of sizes with a characteristic power law, which we show is a consequence of spontaneous coalescence events. These results have implications for the function of nucleoli in ribosome subunit processing and provide a physical link between activity within a macromolecular assembly and its physical properties on larger length scales.

active fluids | cytoskeleton | germinal vesicle | nuclear bodies

A fundamental question in biology is how molecules self-assemble into functional structures with defined three-dimensional architectures. For large assemblies that exhibit defined molecular order, such as ribosomes, quaternary structure formation is determined by stereospecific interactions between subunits. However, the principles that define the size, shape, and dynamics of larger, less-ordered assemblies such as the mitotic spindle or focal adhesions are less clear. RNA/protein bodies that are not membrane delimited constitute a large and important class of intracellular assemblies whose physical properties and assembly pathways are poorly understood. RNA/protein bodies are found in the nucleoplasm and cytoplasm of many cells and play fundamental roles in growth, development, and homeostasis. Their biological importance is underscored by the fact that changes in composition and self-assembly of these structures are associated with devastating diseases including Huntington's (1) and spinal muscular dystrophy (2). Diverse RNA/protein bodies found in the nucleoplasm include nucleoli, Cajal bodies, speckles, and promyelocytic leukemia bodies, among many others (3). They are typically very dynamic at the molecular scale, exchanging subunits with bulk nucleoplasm on a timescale of tens of seconds. Despite elucidation of many molecular biological details, we currently lack a fundamental physical understanding of what holds the RNA and protein components together as a coherent physical structure, how different types of bodies remain distinct from one another, and what sets the size and shape of these structures. Recent evidence suggests that one type of RNA/protein body, called P granules, have liquid-like properties, which can explain the segregation of P granules through development (4). However, whether such liquid properties are a general feature of RNA/protein bodies, and if so what impact this would have on larger-scale properties such as size, shape, and subcellular localization, are unknown.

Nucleoli are essential RNA/protein bodies within the nucleus that function primarily as factories for ribosome subunit biogenesis. Ribosome production is critical for rapid cell growth, and tissue pathologists use the size, number, and shape of nucleoli as indicators of cancer growth and malignancy (5, 6). Nucleoli consist of hundreds of different RNA and protein components, including many ATP-hydrolyzing RNA helicases (7). Ribosome precursors are thought to be assembled and modified during radial transport away from a central core of tandem ribosomal DNA (rDNA) repeats, which are located at positions on chromosomes known as nucleolar organizer regions (NORs). Normal human cells have NORs on five different chromosomes, and can thus have as many as 10 nucleoli; these are readily visualized as phase-dense, often spherical structures within the nucleus. During prophase, large G2 nucleoli disassemble; upon completion of cytokinesis, small nucleoli nucleate and grow on the NORs. These nucleoli increase in size as components continue assembling; moreover, their size appears to increase while their number decreases, probably due to fusion events (8). Nucleolus fusion has not been systematically studied, but it may provide clues to how nucleoli are spatiotemporally organized on supramolecular scales.

The shape and dynamics of somatic nucleoli are strongly influenced by the architecture (9) and transcriptional activity (10) of chromatin. A simpler model system is found in the nucleus [germinal vesicle (GV)] of amphibian oocytes. Amphibian GVs are much larger than somatic nuclei, approximately 0.4–0.5 mm in the *Xenopus laevis* system we use, and the chromatin within them is much more dispersed than in somatic cells. One function of the GV is to provision the egg with large numbers of ribosomes. The mature *X. laevis* GV contains 1,000–1,500 large extrachromosomal nucleoli (Fig. 1*A*) (11); these nucleoli form around cores of tandem rDNA minichromosomes, which split off of chromosomes by a gene amplification process (12, 13). Although nucleoli in GVs are unlike somatic nucleoli in size and number, their function, molecular composition, and structural organization are similar to that of somatic nucleoli (11). Here, we use the GV to probe the mechanochemical nature of nucleoli and elucidate the principles that regulate nucleolar size, shape, and dynamics.

Results

We studied nucleoli in the GV of large *Xenopus* oocytes of diameter 1–1.1 mm, approximately stage V (14). To precisely visualize the shape of nucleoli, we injected mRNA encoding a

Author contributions: C.P.B., T.J.M., and A.A.H. designed research; C.P.B. performed research; T.J.M. and A.A.H. contributed new reagents/analytic tools; C.P.B. analyzed data; and C.P.B., T.J.M., and A.A.H. wrote the paper.

The authors declare no conflict of interest.

This article is a PNAS Direct Submission. D.G. is a guest editor invited by the Editorial Board.

Freely available online through the PNAS open access option.

[1]To whom correspondence should be addressed. E-mail: cbrangwy@princeton.edu.

[2]Present address: Department of Chemical and Biological Engineering, A313 E-quad, Princeton University, Princeton, NJ 08544.

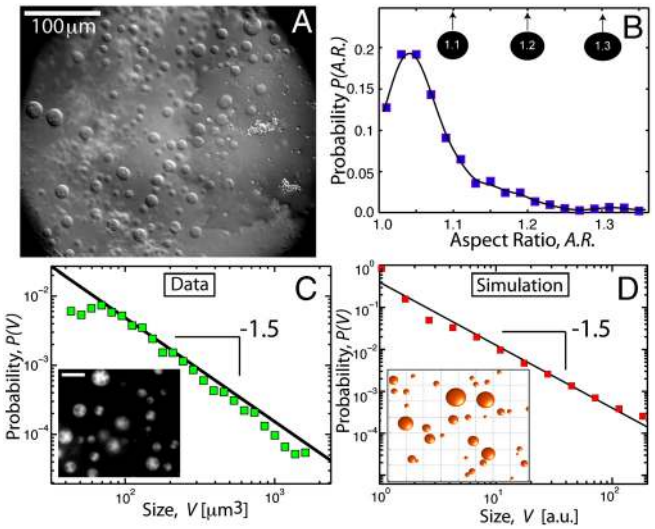

Fig. 1. Size and shape of *X. laevis* oocyte nucleoli. (*A*) DIC image of nucleoli in the *X. laevis* GV. Nuclear bodies can be readily seen in DIC. Most of these are extrachromosomal nucleoli. (*B*) We plot the distribution of nucleolar aspect ratios obtained from analysis of GFP::NPM1 images of nucleoli (*Inset* in *C*). The average is 1.07 ± 0.06; a perfect sphere would be 1.0. Thus, most nucleoli are highly spherical. (*C*) Distribution of nucleolar volume exhibits a power-law distribution with an exponent of −1.5. *Inset* shows an image of GFP::NPM1–labeled nucleoli (scale bar, 20 μm). (*D*) Monte Carlo simulation of fusing droplets, with a slow constant influx of small droplets. The distribution of droplet volume exhibits power-law behavior with an exponent of −1.5. A snapshot of a subregion of the simulation is shown in the *Inset*.

GFP-tagged nucleolar protein, GFP::NPM1, into the oocyte cytoplasm. After overnight incubation, GVs were dissected into mineral oil; under these conditions, nucleoli and other GV contents remained in their native, biosynthetically active state, surrounded by an intact nucleoplasm, and the GV remains viable for several hours (15). NPM1 (nucleophosmin, NO38, B23) localizes to the granular component of nucleoli (16). We observed a distribution of fluorescent, spherical bodies (Fig. 1*C*, *Inset*). Two other tagged nucleolar proteins, GFP::fibrillarin and GFP::NO145, localized to the same bodies, confirming that they are indeed nucleoli (see below). Using custom image analysis routines, we computed their aspect ratio (maximal diameter/minimal diameter). The mean was 1.07 ± 0.06 (mean ± SD, $N = 2859$), indicating a high degree of circularity in optical section (Fig. 1*B*). Because there is no obvious z asymmetry, nucleoli are highly spherical.

Spherical shape could in principle arise from isotropic growth of a solid-like object; this could be expected for nucleoli if some structural RNA and protein components isotropically accumulate around the transcriptional core upon completion of cytokinesis. However, irreversible aggregation would typically result in irregularly shaped assemblies, such as the amyloid plaques seen in the brains of Alzheimer's disease patients (17). An alternative view is that nucleoli represent a dynamic assembly with liquid-like properties, with an effective surface tension that minimizes surface area by viscous relaxation to a spherical shape. Fusion of somatic nucleoli during G1 (discussed above) is more consistent with this physical picture. Moreover, a tendency of liquid-like nucleoli to fuse with one another would lead different sized nucleoli; this would result in a broad size distribution of a particular form, possibly explaining the observation that nucleoli occur in a wide range of sizes, from <1 μm to >10 μm in diameter (18). We determined the size distribution of GFP::NPM1–labeled nucleoli ($N = 2859$). Their volumes, V, fit a power-law distribution, $P(V) \sim V^{\alpha}$, as can be seen by the linear profile on a log–log plot (Fig. 1*C*). The exponent of this distribution was determined to be $\alpha = -1.51 \pm 0.07$. Power-law distributions with an exponent of −1.5 are characteristic of aggregation processes (19, 20). We illustrate this with the result of a simple Monte Carlo simulation, in which there is a constant influx of small droplets, which move by diffusion. When these touch they fuse, leading to larger droplets that diffuse more slowly. This leads to a power-law size distribution, with an exponent of −1.5, as shown in Fig. 1*D*. Thus, large spherical nucleoli may form by fusion of many smaller spherical nucleoli, behaving like liquid droplets.

To test this liquid-like picture, we dissected *Xenopus* GVs into mineral oil and then gently compressed them under a coverslip by approximately 50%, without rupturing the nuclear envelope. Nucleoli in this preparation were often initially nonspherical, apparently due to fusion during sample preparation. When we followed the behavior of nucleoli over time, they often fused with

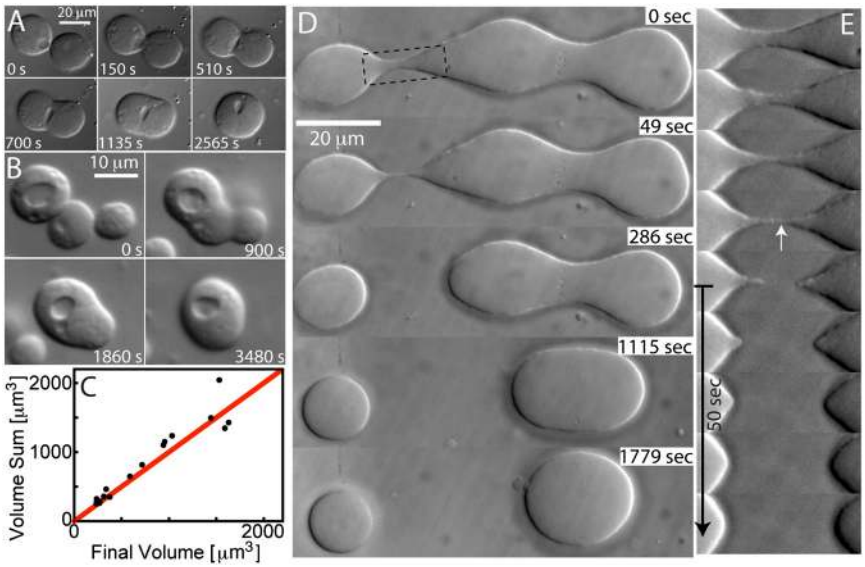

Fig. 2. Fluid-like behavior of nucleoli. (*A*) DIC image sequence showing fusion of two spherical nucleoli into one larger spherical nucleolus. (*B*) DIC image of the fusion of three spherical nucleoli into one larger spherical nucleolus. (*C*) Plot of the sum of nucleoli volumes before and after fusion. The red line corresponds to conserved volume. (*D*) In the first frame, three nucleoli that have come into contact and begun fusing are visible. The bridge between the two on the *Left* is unstable and pinches off, whereas the bridge between the nucleoli on the *Right* is stable and they fuse. (*E*) Close-up of the rupturing bridge from *D*, showing that the threads of nucleolar material are resorbed within 1 min after rupturing.

one another (Fig. 2*A*). The shape of a fusing pair was initially hourglass-like and then relaxed into a sphere over approximately 2,000 s. We frequently observed fusion events involving more than two nucleoli (e.g., three nucleoli fusing in Fig. 2*B*). Typically, every fresh GV preparation contains several fusing nucleoli, allowing us to quantitatively characterize the process for large numbers of fusion events. We first sought to determine whether volume was conserved during fusion, by measuring the diameter of nucleoli before and after fusion, and assuming spherical geometry. We found that volume was conserved during fusion, as shown in Fig. 2*C*. To test the hypothesis that nucleoli are indeed poised to undergo liquid-like fusion upon contact with one another, we used a microneedle to push nucleoli together. We found that when brought into contact, there was typically a delay, which varied from <1 to approximately 5 min, after which nucleoli fused into one larger sphere, as visible in the example shown in Fig. 3.

We never observe fission events in which one nucleolus splits into two or more. However, we occasionally observe two nucleoli that appear to have initiated fusion, but are subsequently pulled apart during sample preparation. In such cases, we observe a characteristic "pinch-off" behavior, in which a slender bridge thins between the two nucleoli, prior to rupturing; liquid bridge rupture is a classic feature of viscous fluids and the subject of much experimental and theoretical study (21). Strikingly, after the bridge ruptures, the two threads rapidly retract and resorb into the body of each of the resulting nucleoli, as shown in Fig. 2 *D* and *E*. This resorption occurred on a timescale of less than 1 min, resulting in a smooth nucleolar surface. These observations show that the nucleolar material exhibits liquid-like behavior even on timescales significantly faster than the several-minute timescale typically required for fusion.

These data suggest that nucleoli indeed exhibit liquid-like viscous relaxation behavior, together with an effective surface tension. This surface tension drives them toward a spherical shape if they are transiently nonspherical, as seen immediately after the onset of fusion. For simple Newtonian liquid drops suspended in a lower viscosity medium, the characteristic time it takes two fusing droplets to assume a spherical shape, τ, is given by $\tau \approx (\eta/\gamma) \cdot \ell$, where η is the drop viscosity, γ is the surface tension, and ℓ is the characteristic length scale (size of drops) (22). We plotted the aspect ratio vs. time of fusing GFP::NPM1–labeled nucleoli (Fig. 4*A*). This was well fit by a simple exponential function, allowing us to determine the characteristic relaxation time τ. We then plotted τ vs. ℓ for a large number of fusion events ($N = 77$). This data showed a roughly linear trend, as for conventional liquids (Fig. 4*B*). The slope gives the ratio of effective nucleolar viscosity to surface tension, known as the inverse capillary velocity, η/γ; from a linear fit we obtain $\eta/\gamma = 46.1$ s/μm. If we assume a typical length scale of $\xi \approx 10$ nm for ribonucleoprotein complexes, from fundamental physical arguments (23) we can estimate that $\gamma \approx \frac{k_B T}{\xi^2} \approx 10$ μN/m. Using the measured capillary velocity, we can thereby estimate the apparent viscosity of nucleoli, of order $\eta_{app} \approx 10^3$ Pa · sec, as shown in Fig. 4*C*. This nucleolar viscosity is 10^6 times larger than water, comparable to that of thick honey; interestingly, it is over an order of magnitude larger than that estimated for P granules in the cytoplasm of *Caenorhabditis elegans* embryos, which are also liquid-like and composed of RNA and protein (4).

In a small number of GV preparations (<5%), nucleoli appeared clumped together, exhibiting irregular shapes that did not relax to spheres over >30 min. In a given preparation, either all contacting nucleoli were spherical and fused, or none were. One possible explanation is that nucleolar fusion depends on active metabolism, and some GVs were damaged so as to inhibit their energy metabolism. To test the role of energy in nucleolar dynamics, we depleted ATP by injecting apyrase into the GV and waiting 30 min before isolation. This enzyme catalyzes ATP hydrolysis and has been shown to strongly deplete ATP in injected GVs (24). The onset of nucleolus fusion was evident in many apyrase-injected GVs, and we were able to collect enough data to study the dynamics of relaxation back to a sphere. The exponential fit of the aspect ratio vs. time was not as good as for untreated or buffer-injected GVs and exhibited significantly more scatter in plots of τ vs. ℓ. On average, ATP-depleted oocytes exhibited distinctly slower relaxation dynamics, with a higher inverse capillary velocity $\eta/\gamma = 584 \pm 803$ s/μm ($N = 46$). Using the estimate $\gamma \approx 10$ μN/m as above, this suggests ATP-depleted nucleoli exhibit an apparent viscosity approximately 10-fold larger than untreated nucleoli (Fig. 4 *B* and *C*).

A large number of studies using electron microscopy and fluorescence-based imaging of nucleoli has shown that they are not homogenous droplets, but rather exhibit a complex core-shell structure (7). This finding is inconsistent with a simple liquid-like picture in which internal contents would mix. To address this, we visualized nucleolar substructure during fusion events. Within the nucleolus, newly transcribed rRNAs are found in a core known as the dense fibrillar component, and fibrillarin is one of a large subclass of nucleolar proteins that specifically localize to this core region. We injected mRNA encoding GFP-tagged fibrillarin to

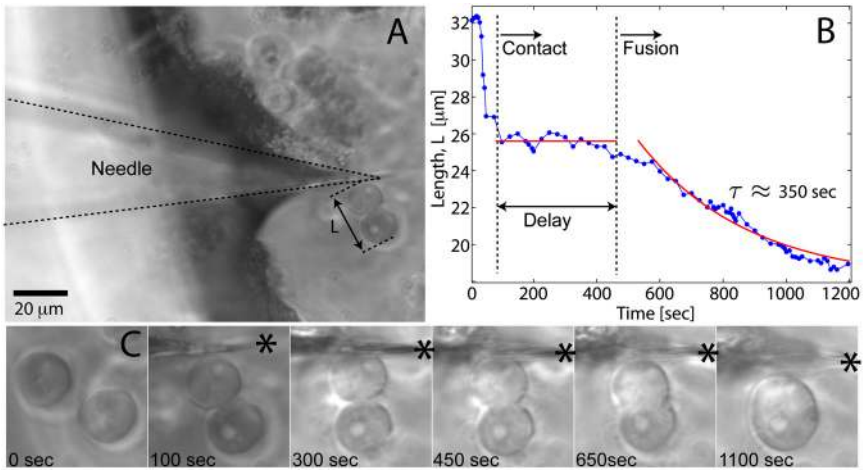

Fig. 3. Needle-induced fusion of two nucleoli. (*A*) Image showing a microneedle that has been used to move two nucleoli together. (*B*) Time course of the distance between the two nucleoli. Initially they are not touching. At approximately 75 s, they are brought into contact with one another, but they do not appear to begin fusing until approximately 500 s, when they fuse into a single round sphere on a timescale of $\tau \sim 350$ s. (*C*) Images showing the sequence of events. The needle is visible in the second frame (needle tip position denoted by the asterisk).

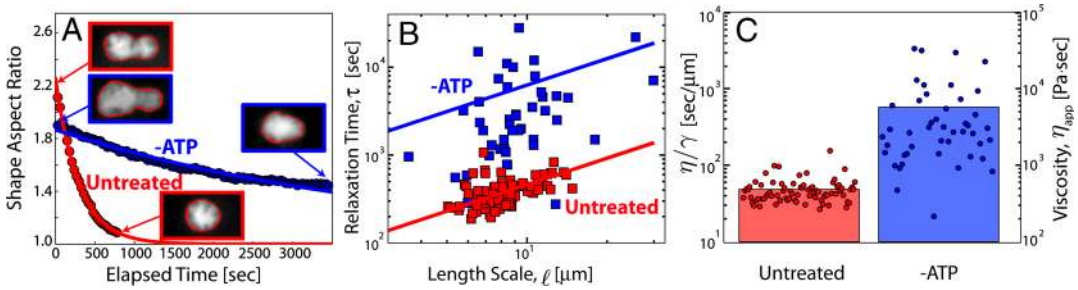

Fig. 4. Analysis of fusion dynamics and ATP dependence. (*A*) The red curve shows the dynamics of a single example control fusion event of two GFP::NPM1–labeled nucleoli, shown by the images in the red box. The blue curve shows the slower fusion dynamics of a comparable pair of GFP::NPM1 nucleoli (blue boxes) in an ATP-depleted GV. The red outline in the images is the output of the image analysis routines used to calculate aspect ratio. (*B*) Plot of the fusion time, τ, vs. length, ℓ, from untreated nucleoli ($N = 77$), and apyrase-treated nucleoli ($N = 46$). The red and blue lines are linear fits to the control and apyrase data, respectively. (*C*) Scatter plot of η/γ obtained from control and ATP-depleted nucleoli. The *Right* axis reflects the apparent viscosity, η_{app}, obtained assuming a surface tension of $\gamma = 10$ μN/m.

observe the structure and dynamics of GFP::fibrillarin cores. Consistent with large nucleoli arising from fusion of several smaller nucleoli, large nucleoli always contained multiple GFP::fibrillarin cores, whereas the smallest nucleoli contained only one core (Fig. 5*A*). We followed the dynamics of these fibrillarin cores during fusion events. Occasionally, the cores appear to fuse with one another, but typically they remained as distinct subnucleolar structures (Fig. 5*B*). Thus, larger nucleoli formed by multiple fusion events tended to accumulate a roughly additive number of cores. The nucleolar protein NO145 localizes to a cortical shell (25), which could present a barrier to nucleolar fusion. In GFP::NO145-expressing GVs, the shell was readily visualized (Fig. 5 *C* and *D*). It appeared to rapidly restructure during nucleolar fusion (Fig. 5*C*). This is consistent with our observation from movies that there is no, or only a small, kinetic barrier to nucleolar fusion. Interestingly, GFP::NO145 also localized to the surface of spheroidal structures within nucleoli that appear to contain nucleoplasm (Fig. 5*D*). Thus, the behavior of NO145 is analogous to that of a surfactant, coating any interface between the nucleolar granular component and the nucleoplasm.

GVs in *X. laevis* ooctyes typically contain more than 1,000 nucleoli. Because nucleoli that contact each other fuse, it is unclear what keeps them from all fusing into a single large body during the weeks-long growth of the oocyte in the ovary. Using micromanipulation, we observed evidence for some elastic scaffold surrounding nucleoli within the GV. When we pulled on one internal region of the GV, nucleoli in distant regions (>100 μm away) were observed to become displaced and deformed, as shown in Fig. 6*A*. Actin is present in abundance in the GV nucleus, where an f-actin network is thought to maintain GV structural stability (26) and perhaps also to guide RNA transport (27). To test if an actin-based elastic scaffold slows internal mobility and thus internucleolar contact, we treated GVs with the f-actin-disrupting drug Cytochalasin D (Cyto-D) (Fig. 6*B*). We find that in Cyto-D–treated GVs, large numbers of nucleoli fused into one large mass over the course of approximately 30 min, as shown in the sequence in Fig. 6*B*. However, these fusion events appear qualitatively different from fusion seen in unperturbed embryos (e.g., Figs. 2 and 3). In particular, fusion was frequently incomplete. Perhaps, in the absence of actin filaments, nucleolar substructures are incapable of undergoing the structural rearrangements necessary to completely self-assemble into one larger nucleolus.

Discussion

In this study, we show that nucleoli behave as liquid-like droplets, and that this feature can explain both their spherical shape and their broad, power-law size distribution in amphibian oocytes. It can also explain how nucleoli in somatic cells fuse, a behavior first described over 100 years ago (see ref. 28 and references therein). Our findings are broadly consistent with a previous study suggesting that nucleoli and other nuclear bodies have a low-density, sponge-like structure (29); however, our findings show that this sponge-like structure must be able to flow as a liquid on a timescale of tens of seconds. Given its fluid-like behavior, the nucleolus, particularly the granular component of the nucleolus, cannot be a structurally well-defined assembly of macromolecules on large length scales >100 nm; they presumably do exhibit defined molecular interactions on the nanometer scale. These observations, combined with most nucleoli containing multiple transcriptional cores (Fig. 5), are at odds with the concept of an ordered, vectoral assembly pathway initiated from one central site of active transcription (30). Rather, transcription sites may act as nuclei for condensation of nucleolar material as small droplets, which can readily fuse with neighboring droplets.

Our results paint the amphibian GV as an emulsion of liquid-like nucleolar droplets suspended in bulk nucleoplasm, which is infiltrated by actin filaments that seem to partially immobilize nucleoli. Power-law size distributions with an exponent of −1.5, like that we describe here, can occur in aggregation systems

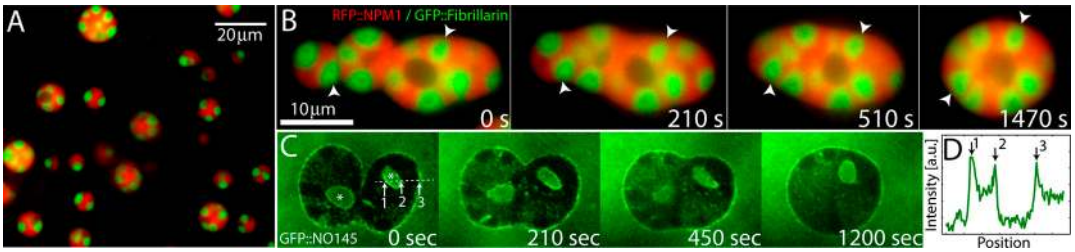

Fig. 5. Dynamics of nucleolar substructures. (*A*) A GV exhibiting GFP::fibrillarin/RFP::NPM1–labeled nucleoli. Note that larger nucleoli contain many fibrillarin cores, whereas smaller nucleoli contain only one or two fibrillarin cores. (*B*) Image sequence showing fusion of several GFP::fibrillarin/RFP::NPM1-labeled nucleoli. Arrowheads track the positions of two fibrillar cores. (*C*) Image sequence showing the dynamics of GFP::NO145 at the cortex of two fusing nucleoli. Note the GFP::NO145 localization to the interior of nucleoli at the surface of nucleolar vacuole-like structures (*). (*D*) Intensity profile across the dotted line shown in *C*; peaks 1 and 2 reflect vacuolar surface, and peak 3 reflects nucleolar cortex.

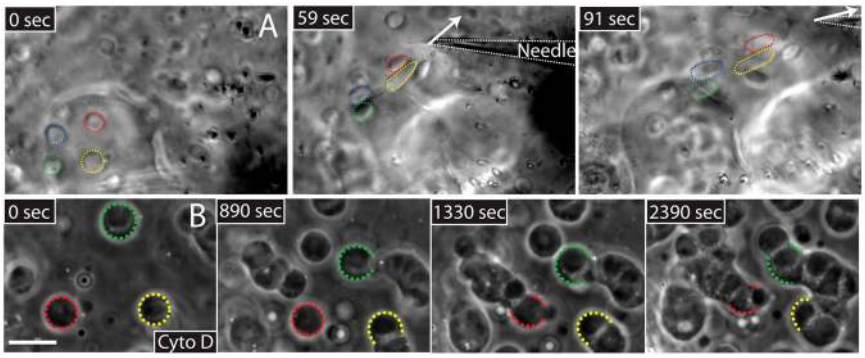

Fig. 6. The role of a surrounding actin scaffold in slowing internucleolar contact. (*A*) Pulling on one region of the GV with a microneedle displaces nucleoli in distal regions, suggesting the presence of an elastic scaffold. Four nucleoli are highlighted. (*B*) GV treated with Cyto-D to disrupt filamentous actin. Nucleoli freely diffuse throughout the GV and fuse with one another upon contact; the fates of three nucleoli are highlighted. One large nucleolar clump results; note, however, that under these drug conditions nucleoli do not appear to regain sphericity and fusion appears perturbed.

without a constant influx of elementary particles (19). However, the slow diffusivity and limited barrier to fusion upon contact suggest that our system is clearly in a diffusion-limited regime; for such a system, a constant particle influx is necessary to exhibit a power law with exponent −1.5, a result that is robust in two and three dimensions (20, 31). We thus hypothesize that the nucleolar size distribution is determined by both the rate of production of amplified rDNA minichromosomes, and the rate at which nucleoli contact one another. Turnover and relaxation dynamics of the f-actin network likely set the rate at which the embedded nucleoli diffuse, and thereby contact one another and fuse (Fig. 6 *C* and *D*). Upon Cyto-D treatment, GV fusion appears perturbed (Fig. 6*B*), and it is possible that the surrounding f-actin network could also contribute to setting the relaxation timescale of fusing nucleoli; however, under these conditions the fusion timescales do not appear to be significantly increased as would be expected if f-actin relaxation was dominant.

We do not yet understand if there is a functional significance of nucleolar fusion, or whether the resulting power-law size distribution is advantageous. Power-law distributions have the unique property of being "scale-free" (32), which in this context means that there is no characteristic nucleolar size. Nucleolar size determines the surface/volume ratio, and this may influence the rate at which components are exchanged with the nucleoplasm. Surfactants can greatly influence the rate of material exchange at interfaces, which is an interesting putative function for NO145 and similar proteins.

The nucleolus is only one type of a large number of RNA/protein bodies that are found throughout the nucleoplasm and cytoplasm, including germ granules (33), processing bodies (34), and Cajal bodies (2), all of which tend to be spherical in shape. Germ granules in *C. elegans* embryos (P granules) were previously shown to exhibit liquid-like properties, using observations similar to those we report here (4). Our finding that nucleoli also behave as liquid drops suggests that this could be a common feature of RNA/protein assemblies, which has important implications for their function. Liquid-like subcompartments facilitate the concentration of components, while maintaining molecular mobility, thus functioning as small reaction compartments. Within these compartments, the concentration of certain molecules, otherwise too dilute, can far exceed their binding constants.

ATP depletion with apyrase caused nucleoli to exhibit approximately 10-fold increase in apparent viscosity, almost to the point of "freezing." This suggests that active, dissipative processes—for example, helicase activity—play a role in internal structural reorganizations that promote liquidity. The GV nucleoli studied here are highly spherical; however, nucleoli in some systems are nonspherical, including amphibian GV nucleoli from earlier stages (35). Our findings that there is an ATP dependence to the liquid-like behavior underlying spherical shape suggests that nonspherical nucleoli could reflect altered metabolic activity. Indeed, there is an intimate but still poorly understood connection between the size and shape of nucleoli and the metabolic state of cells (36). Moreover, irregular shapes are typical of stress granules (37), RNA/protein bodies that form in response to environmental stresses, including metabolic stress. Interestingly, purified nucleoli from lysed HeLa cell nuclei were reported to be nonspherical and did not fuse, even while retaining function by the criterion of transcribing when ATP was added (38). We suspect fusion may require dynamic exchange of subunits between nucleoli and bulk nucleoplasm as well as ATP hydrolysis, and these collective molecular dynamics that give rise to the liquidity will be severely perturbed when nucleoli are isolated into buffer alone. Lack of molecular turnover and liquidity—i.e., freezing—may account for the success of nucleolus purification protocols. In any case, the findings we report here suggest that dynamic, metabolically active nucleoli exhibit a driving force toward a spherical shape that appears to be altered in nonspherical nucleoli and stress granules. Further study will be required to elucidate the precise molecular components involved in sculpting the shape of nucleoli and other active macromolecular assemblies.

Materials and Methods

Ooctye Preparation. Oocytes were surgically removed from adult female *X. laevis* frogs that had been anesthetized for 20 min in 0.1% Tricaine (Sigma), 25 mM $NaHC0_3$. Oocytes were incubated overnight at 20 °C in OR2 (29). The next day, oocytes were partially mechanically separated with forceps and then defolliculated by gentle rocking for 30–50 min in 2 mg/mL collagenase (Sigma) in OR2. Collagenase-treated oocytes were injected with mRNA encoding GFP-tagged or red fluorescent protein (RFP)-tagged nucleolar proteins. After overnight incubation at 20 °C, GVs were removed in oil and imaged.

DNA Constructs and mRNA. All DNA constructs used in this study were cloned using either a C-terminal EGFP–pCS2+ vector, or a C-terminal RFP-pCS2+ vector (gift of C.P. Heisenberg). An EGFP::NPM1 construct was cloned using a cDNA encoding the *X. laevis* NPM1 gene (clone IRBHp990F028D, Imagene), which was PCR amplified with an N-terminal Xho1 endonuclease site and a C-terminal XmaI site. An rfp::NPM1 construct was cloned by PCR amplifying this cDNA with an N-terminal EcoRI site and a C-terminal XhoI site. An EGFP::no145 construct was cloned using a cDNA encoding the *X. laevis* no145 gene (clone MGC:179985, Imagene), which was PCR amplified with an N-terminal Xho1 site, and a C-terminal XmaI site. An EGFP::fibrillarin construct was cloned using a cDNA encoding the *Xenopus tropicalis* fibrillarin gene (clone MGC76139, Imagene), which was PCR amplified with an N-terminal XhoI site, and a C-terminal XmaI site. For each of these constructs, mRNA was generated by first linearizing the pCS2+ vector at the NotI site, and then using an in vitro SP6-based capped RNA transcription kit (mMessage mMachine, Ambion). Transcribed mRNA was purified using RNeasy spin columns (Qiagen), and injected (approximately 10 nL) into the cytoplasm of defolliculated oocytes.

Microscopy, Microinjection, and Micromanipulation. Differential interference contrast (DIC) and fluorescence microscopy were performed using a standard widefield epifluorescence Zeiss inverted microscope equipped with a Hamamatsu Orca CCD camera, and a 20× dry and 63× oil-immersion objective. Microinjection was performed using an Eppendorf Transjector coupled to a Zeiss dissecting microscope. Micromanipulation was performed using an Eppendorf micromanipulator mounted on a Zeiss Axiovert inverted microscope.

ATP-Depletion Experiments. The GVs of defolliculated oocytes were injected with approximately 500 pL 2 mg/mL Apyrase (Sigma) dissolved in H_2O. To verify that GVs had been injected, 20–100 nm blue fluorescent beads were included in the injection mix. After >30 min incubation, GVs were dissected into oil. We verified that the small amount of injected H_2O (approximately 1% of GV volume) had no effect on the timescales of nucleolar fusion events. To determine ATP concentration, untreated and Apyrase-injected GVs were mixed into a luciferase solution using an ATP determination kit (Invitrogen). ATP-dependent luminescence was determined using a GENios Pro luminometer (Tecan). ATP concentration was approximately 10-fold lower in apyrase-injected GVs.

Nucleolar Size and Shape Analysis. For both nucleolar size determination and aspect ratio measurements, GFP::NPM1–labeled nucleoli were imaged using a 20× objective. Image analysis routines were written in Matlab. Volume was calculated from the area of nucleoli determined from above threshold pixels. Out-of-focus nucleoli were discarded from analysis. A total of 2,859 nucleolar volumes were binned logarithmically such that bin widths are uniformly sized on a logarithmic plot, and transformed to probabilities by normalizing to the bin widths. Using Matlab fitting routines, the probability distribution was fit to a power law of the form $P(V) = C \cdot V^{\alpha}$. The R^2 value of the fit was maximized by excluding the first three data points, which are subject to increased experimental error due to intrinsic noise limitations. Error bars are 95% confidence intervals.

The aspect ratio, A.R., of nucleoli was determined by fitting an ellipse to the shape and calculating A.R. $= \ell_{\text{long}}/\ell_{\text{short}}$, where ℓ_{long} and ℓ_{short} are the long and short axes of the ellipse. For analysis of fusing nucleoli, the time evolution of this aspect ratio was fit to a function of the form A.R. $= 1 + (\text{A.R.}_0 - 1) \cdot \exp(-t/\tau)$, where t is time, τ is the characteristic relaxation time, and A.R._0 is the initial aspect ratio. We define the length scale of these fusing nucleoli as a geometric mean $\ell = [(\ell_{\text{long}}(t = 0) - \ell_{\text{short}}(t = 0)) \cdot \ell_{\text{short}}(t = 0)]^{1/2}$. Plots of τ vs. ℓ were fit to a line of the form $\tau = (\eta/\gamma) \cdot \ell$, to determine the inverse capillary velocity η/γ.

Monte Carlo Simulation. To illustrate the emergence of a power-law size distribution in a collection of fusing particles, we developed a simple Matlab-based simulation. We began the simulation with 5,000 particles, uniformly of radius a_0, distributed in a 2D simulation volume of size $b \times b$ with reflecting boundary conditions. The diffusion coefficient of droplets is given by the Stokes–Einstein relation, $D = \frac{k_B T}{6\pi\eta_{\text{med}} a}$, where $k_B T$ is the thermal energy scale, η_{med} here is the viscosity of the surrounding medium, and a is the radius of the droplet. At each time step, Δt, a particle moves by an amount $(4D\Delta t)^{1/2} \cdot \xi$, where ξ is a normally distributed random variable with mean 0 and standard deviation 1. Particles that overlap are fused into a larger particle, conserving volume. At each time step we introduce a small number, J, of single particles into the simulation volume. After a large number of simulation timesteps (typically about 10^4–10^5), an apparent quasi-steady-state droplet size distribution is reached; for a broad distribution of parameters, a power-law size distribution results, with an exponent of −1.5.

ACKNOWLEDGMENTS. We thank Joe Gall for initially showing us how to work with the *Xenopus* GV. We thank Patricia Heyn and C.P. Heisenberg for sharing reagents, Andrei Pozniakovsky for invaluable help with cloning, Heino Andreas, Jorge Contreras, and Agenor Limon for help with frog husbandry and oocyte preparation, and Peter Pitrone and members of the Max Planck Institute of Molecular Cell Biology and Genetics Light Microscopy Facility, as well as the Nikon Imaging group at Marine Biological Laboratory, for microscopy assistance. Thanks to Christian Eckmann, Karla Neugebauer, Frank Jülicher, Jonathan Dawson, Jöbin Gharakhani, and members of the Max Planck Institute for the Physics of Complex Systems and Max Planck Institute of Molecular Cell Biology and Genetics for helpful discussions. C.P.B. was supported by a fellowship from the Helen Hay Whitney Foundation.

1. Savas JN, et al. (2008) Huntington's disease protein contributes to RNA-mediated gene silencing through association with Argonaute and P bodies. *Proc Natl Acad Sci USA* 105:10820–10825.
2. Gall JG (2000) Cajal bodies: The first 100 years. *Annu Rev Cell Dev Biol* 16:273–300.
3. Spector DL (2001) Nuclear domains. *J Cell Sci* 114:2891–2893.
4. Brangwynne CP, et al. (2009) Germline P granules are liquid droplets that localize by controlled dissolution/condensation. *Science* 324:1729–1732.
5. Helpap B (1988) Observations on the number, size and localization of nucleoli in hyperplastic and neoplastic prostatic disease. *Histopathology* 13:203–211.
6. Derenzini M, et al. (2000) Nucleolar size indicates the rapidity of cell proliferation in cancer tissues. *J Pathol* 191:181–186.
7. Boisvert FM, van Koningsbruggen S, Navascues J, Lamond AI (2007) The multifunctional nucleolus. *Nat Rev Mol Cell Biol* 8:574–585.
8. Anastassova-Kristeva M (1977) The nucleolar cycle in man. *J Cell Sci* 25:103–110.
9. Maniotis AJ, Chen CS, Ingber DE (1997) Demonstration of mechanical connections between integrins, cytoskeletal filaments, and nucleoplasm that stabilize nuclear structure. *Proc Natl Acad Sci USA* 94:849–854.
10. Shav-Tal Y, et al. (2005) Dynamic sorting of nuclear components into distinct nucleolar caps during transcriptional inhibition. *Mol Biol Cell* 16:2395–2413.
11. Gall JG, Wu Z, Murphy C, Gao H (2004) Structure in the amphibian germinal vesicle. *Exp Cell Res* 296:28–34.
12. Gall JG (1968) Differential synthesis of the genes for ribosomal RNA during amphibian oogenesis. *Proc Natl Acad Sci USA* 60:553–560.
13. Brown DD, Dawid IB (1968) Specific gene amplification in oocytes. Oocyte nuclei contain extrachromosomal replicas of the genes for ribosomal RNA. *Science* 160:272–280.
14. Dumont JN (1972) Oogenesis in Xenopus laevis (Daudin). I. Stages of oocyte development in laboratory maintained animals. *J Morphol* 136:153–179.
15. Paine PL, Johnson ME, Lau Y-T, Tluczek LJM, Miller DS (1992) The oocyte nucleus isolated in oil retains in vivo structure and functions. *Biotechniques* 13:238–246.
16. Peculis BA, Gall JG (1992) Localization of the nucleolar protein NO38 in amphibian oocytes. *J Cell Biol* 116:1–14.
17. Mathis CA, Wang Y, Klunk WE (2004) Imaging beta-amyloid plaques and neurofibrillary tangles in the aging human brain. *Curr Pharm Design* 10:1469–1492.
18. Wu Z, Gall JG (1997) "Micronucleoli" in the Xenopus germinal vesicle. *Chromosoma* 105:438–443.
19. Weitz DA, Lin MY (1986) Dynamic scaling of cluster-mass distributions in kinetic colloid aggregation. *Phys Rev Lett* 57:2037–2040.
20. Huber G (1991) Scheidegger's rivers, Takayasu's aggregates and continued fractions. *Physica A* 170:463–470.
21. Stone HA (1994) Dynamics of drop deformation and breakup in viscous fluids. *Annu Rev Fluid Mech* 26:65–102.
22. Eggers J, Lister JR, Stone HA (1999) Coalescence of liquid drops. *J Fluid Mech* 401:293–310.
23. Aarts DG, Schmidt M, Lekkerkerker HN (2004) Direct visual observation of thermal capillary waves. *Science* 304:847–850.
24. Bataille N, Helser T, Fried HM (1990) Cytoplasmic transport of ribosomal subunits microinjected into the Xenopus laevis oocyte nucleus: A generalized, facilitated process. *J Cell Biol* 111:1571–1582.
25. Kneissel S, et al. (2001) A novel karyoskeletal protein: Characterization of protein NO145, the major component of nucleolar cortical skeleton in Xenopus oocytes. *Mol Biol Cell* 12:3904–3918.
26. Bohnsack MT, Stuven T, Kuhn C, Cordes VC, Görlich D (2006) A selective block of nuclear actin export stabilizes the giant nuclei of Xenopus oocytes. *Nat Cell Biol* 8:257–263.
27. Gounon P, Karsenti E (1981) Involvement of contractile proteins in the changes in consistency of oocyte nucleoplasm of the newt Pleurodeles waltlii. *J Cell Biol* 88:410–421.
28. Amenta PS (1961) Fusion of nucleoli in cells cultured from the heart of Triturus viridescens. *Anat Rec* 139:155–165.
29. Handwerger KE, Cordero JA, Gall JG (2005) Cajal bodies, nucleoli, and speckles in the Xenopus oocyte nucleus have a low-density, sponge-like structure. *Mol Biol Cell* 16:202–211.
30. Olson MO, Dundr M (2005) The moving parts of the nucleolus. *Histochem Cell Biol* 123:203–216.
31. Takayasu H, Nishikawa II, Tasaki H (1988) Power-law mass distribution of aggregation systems with injection. *Phys Rev A* 37:3110–3117.
32. Newman MEJ (2005) Power laws, Pareto distributions and Zipf's law. *Contemp Phys* 46:323–351.
33. Strome S, Lehmann R (2007) Germ versus soma decisions: Lessons from flies and worms. *Science* 316:392–393.
34. Sheth U, Parker R (2003) Decapping and decay of messenger RNA occur in cytoplasmic processing bodies. *Science* 300:805–808.
35. Lane NJ (1967) Spheroidal and ring nucleoli in amphibian oocytes. Patterns of uridine incorporation and fine structural features. *J Cell Biol* 35:421–434.
36. Malatesta M, et al. (2000) Nucleoli undergo structural and molecular modifications during hibernation. *Chromosoma* 109:506–513.
37. Souquere S, et al. (2009) Unravelling the ultrastructure of stress granules and associated P-bodies in human cells. *J Cell Sci* 122:3619–3626.
38. Andersen JS, et al. (2005) Nucleolar proteome dynamics. *Nature* 433:77–83.